JOURNAL OF THERMOPHYSICS AND HEAT TRANSFER
Vol. 16, No. 1, January–March 2002

Generalized Model for Infrared Perception from an Engine Exhaust

Srinath S. Heragu* and K. V. L. Rao†
Aeronautical Development Agency, Bangalore 560 037, India
and
B. N. Raghunandan‡
Indian Institute of Science, Bangalore 560 012, India

A comprehensive scheme has been developed for the prediction of radiation from engine exhaust and its incidence on an arbitrarily located sensor. Existing codes have been modified for the simulation of flows inside nozzles and jets. A novel view factor computation scheme has been applied for the determination of the radiosities of the discrete panels of a diffuse and gray nozzle surface. The narrowband model has been used to model the radiation from the gas inside the nozzle and the nonhomogeneous jet. The gas radiation from the nozzle inclusive of nozzle surface radiosities have been used as boundary conditions on the jet radiation. Geometric modeling techniques have been developed to identify and isolate nozzle surface panels and gas columns of the nozzle and jet to determine the radiation signals incident on the sensor. The scheme has been validated for intensity and heat flux predictions, and some useful results of practical importance have been generated to establish its viability for infrared signature analysis of jets.

Nomenclature

A_1, A_2	=	surface areas in view factor geometry
a_G, a_λ	=	absorption coefficients of gray gas and real gas
C	=	carbon dioxide concentration
C_c	=	carbon dioxide concentration at nozzle axis
(C_x, C_y, C_z)	=	sensor center
D_e	=	nozzle exit diameter
$D(K)$	=	discrete elemental distances along jet axis
$\mathrm{d}A_j, \mathrm{d}A_k$	=	elemental areas of panels j and k
$\mathrm{d}A_s$	=	elemental area projected onto hemisphere surface
$\mathrm{d}a, \mathrm{d}A_b$	=	elemental area of sensor and elemental area projected onto base of hemisphere
$\mathrm{d}F_{dj-dk}$	=	elemental view factor between elemental surface j and elemental surface k
$\mathrm{d}q_{\lambda I,k}, \mathrm{d}q_{\lambda O,k}$	=	elemental incoming and outgoing spectral heat fluxes of panel k
$\mathrm{d}\lambda$	=	elemental wavelength
$\mathrm{d}\omega_j, \mathrm{d}\omega_k$	=	elemental solid angles
(E_x, E_y, E_z), (E_{x1}, E_{y1}, E_{z1})	=	centroids of panels
$e_{\lambda B,G}$	=	blackbody spectral emissive power corresponding to gas temperature inside nozzle
$e_{\lambda B,k}$	=	blackbody spectral emissive power corresponding to T_k
F_{1-2}	=	view factor from area A_1 to A_2
h	=	distance between surfaces in view factor geometry
i'_λ, i'_ω	=	spectral intensities based on wavelength and wave number
$i'_{\lambda b}, i'$	=	blackbody spectral intensity and total intensity
$i'_\lambda(O)$	=	spectral intensity incident on gas column
$i'_{\lambda O,j}$	=	spectral radiosity of panel j
k_g	=	number of jet sections
L_N	=	idealized nozzle length
M_e	=	nozzle exit Mach number
N_{dg}, N_{sg}	=	number of radial sectors and even number of angular sectors of nozzle face and subsequent jet sections
$P(I)$	=	jet cross section radii at discrete elemental distances $D(K)$
(P_{ag}, Q_{ag}, R_{ag})	=	point on the engine side of nozzle axis
(P_{cg}, Q_{cg}, R_{cg})	=	center of nozzle exit face
(P_x, P_y, P_z)	=	point on perpendicular to the sensor on its active side
p', p'_e, p'_0	=	static pressure, nozzle exit pressure and stagnation pressure
q	=	heat flux per unit area
q^*	=	nondimensional form of heat flux, $q/(\sigma \times 100^4)$
R_j	=	radius of jet section
r	=	distance along line of sight from far end to sensor center
r_s	=	radius of sphere in view factor computation by unit sphere method
r_1, r_2	=	radii of disks in view factor geometry
s	=	length of gas column or distance between centroids of panels j and k
$T', T'_{\mathrm{amb}}, T'_c$	=	static temperature, ambient temperature, and axial temperature
T'_e, T'_0	=	nozzle exit temperature and stagnation temperature
U', U'_c, U'_e	=	x component of velocity, axial velocity, and nozzle exit velocity
X_i	=	optical path length of species i
(X_{cg}, Y_{cg}, Z_{cg})	=	point on the edge of nozzle exit face
x	=	axial or curvilinear coordinate
(x_{n1}, y_{n1}, z_{n1}), (x_{n2}, y_{n2}, z_{n2}), (x_{n3}, y_{n3}, z_{n3})	=	vertices of panel

Received 6 November 2000; revision received 25 May 2001; accepted for publication 29 May 2001.

*Scientist, Signature Studies Group.
†Project Director, Propulsion Systems.
‡Professor, Department of Aerospace Engineering.

(x_{t1}, y_{t1}, z_{t1}), (x_{t2}, y_{t2}, z_{t2}), (x_{t3}, y_{t3}, z_{t3}) = projections of panel vertices onto hemisphere base
α = angle between sensor perpendicular and line joining sensor center with panel centroid
$\alpha_{\lambda, j-k}$ = spectral absorptivity of gas column between panels j and k
β = angle between perpendicular to panel and line joining panel centroid with sensor
$\in_k, \rho_k$ = emissivity and reflectivity of panel k
θ_j, θ_k = angles between perpendiculars to panels j and k with the line joining the centers of these panels
λ, ω = wavelength and wave number
τ_λ = spectral transmissivity
$\tau_{\lambda, j-k}$ = spectral transmissivity of gas column between panels j and k
ϕ = angle between nozzle axis and line joining nozzle exit face center to sensor center

Introduction

PRESENT day aircraft detection technologies have advanced from active detection to passive detection and enable detection in an almost all round spherical envelope. Thus stealth, as determined by the various signatures such as acoustic, visible, infrared (IR), and radar, has become an integral part of modern aircraft design. IR signature has assumed importance because it enables passive detection. The aircraft surfaces radiate predominately in the 8–14 μm band whereas the engine exhaust or jet radiates strongly in the 2–6 μm band. The jet radiation, which is the primary source of IR, especially in afterburning mode, depends on its size, shape, and species composition and is also influenced by the radiation from the nozzle interior. This nozzle radiation is determined by the characteristics of its surface in terms of geometry, texture, and temperature and the hot combustion gases contained by it. The radiation from the exhaust is to some extent governed by the nature of expansion, but the increasing use of a variable convergent–divergent nozzle should allow for optimum flow expansions for almost all flight conditions.

A search of literature reveals that this problem of jet radiation most often has been addressed from an academic viewpoint only and not in its totality. Many researchers have dwelt either on the radiation inside the enclosure or the outside gas radiation separately, whereas no one has considered the practically important aspect of the arbitrary location and orientation of the sensor.

One of the earliest methods for solution of radiative transfer in enclosures is Hottel and Sarofim's zone method,[1] applicable for nonisothermal gas environments inside arbitrarily shaped enclosures. Lockwood and Shah[2] developed a method known as the discrete transfer method for the analysis of thermal radiation in combustors. It combines features and advantages of Hottel and Sarofim's zone method,[1] Monte Carlo method,[3] and flux models[4,5] while avoiding their shortcomings. However the assumption of a constant absorption coefficient for the gas may limit its practical utility. Chui et al.[6] presented a finite volume method (FVM) for three-dimensional radiation problems in cylindrical enclosures. Accurate predictions made for benchmark real furnace problems make this a good test for validation. Chai et al.[7] extended the FVM for a Cartesian coordinate system to model irregular geometries for participating media and walls using body-fitted coordinates. The predictions show good agreement with established results. However, the solutions given by Chui et al.[6] and Chai et al.,[7] though applicable for absorbing, emitting, and scatterring media, have limited practical utility due to a gray gas assumption.

Decher[8] analyzed IR emission characteristics using a simple absorption coefficient model, for an ideal cycle of a mixed flow turbofan having a rectangular nozzle to aid in the selection of candidate designs. He indicated that the parameters that increase efficiency reduce IR emissions and that the increase in IR emissions due to afterburning are quite large compared to the corresponding thrust augmentation.

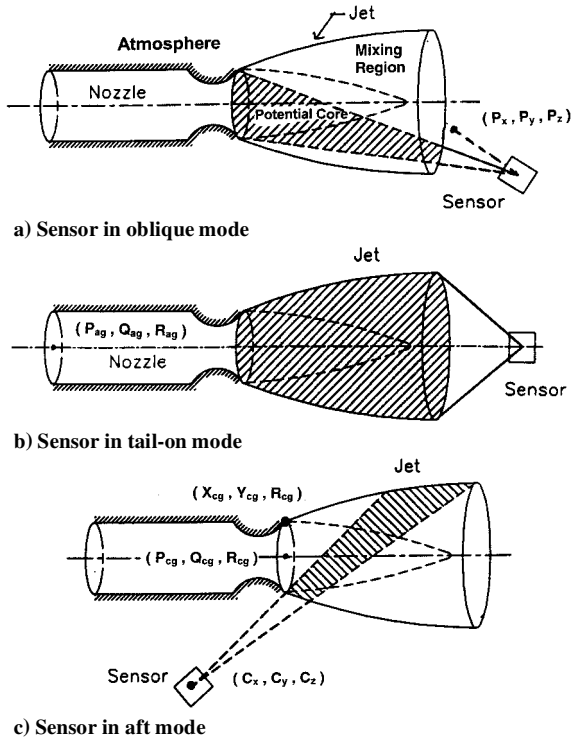

Fig. 1 Sensor location relative to jet.

Gauffre[9] presented cursory details of a comprehensive package for the IR radiation modeling of a full aircraft in the presence of a participating atmosphere. Though no experimental validation has been presented, the effort can be considered as a significant step in the total solution process where the essentials of IR radiation have been achieved. The physical limitations present in radiative studies were removed to a large extent by Ludwig et al.,[10] who presented a theoretical model and some experimental validation for spectral radiance calculation of nonhomogeneous media with a cylindrical configuration. The band model formulated in this work has been adopted by many.

Docherty and Fairweather[11] adapted the discrete transfer method, compatible with finite difference methods, to provide a computationally inexpensive prediction procedure based on the proven ability of the exponential wideband model of Edwards[12] to describe radiative transfer in nongray systems that may contain soot. The predictions made by this method for representative one-dimensional fire configurations compare well with the predictions of a narrowband statistical model. In addition, the effect of soot and path length on the radiative intensity, the directional bias of radiation of asymmetrical profiles, and the dominance of gaseous species or soot on radiation are demonstrated.

Radiation from hot jets is complicated in terms of radiation from the nozzle, noncylindrical hot gas core, unconfined nature, and the consequent mixing processes and the geometric orientation and location of the surface at which the IR intensity or heat flux is to be estimated, as shown in Fig. 1. These have not been considered so far in literature. This paper deals with the IR signature of an optimally expanded circular jet and is an ab initio modeling of gas radiation in combination with geometric modeling.

The aim of this paper is to predict and simulate the radiation levels on an arbitrarily located and oriented sensor from an engine exhaust jet inclusive of the contribution from the nozzle interior. It is generally perceived that a missile, during the initial part of its trajectory, looks at the target emitting IR radiation, as a hot source, whereas at close distances, the target radiation is perceived in greater detail as a combination of hot sources and is used to guide the missile or trigger the warhead. The detailed modeling that has been developed in the present work is very appropriate to near range applications of present day all aspect missiles and is naturally valid for long distances, too.

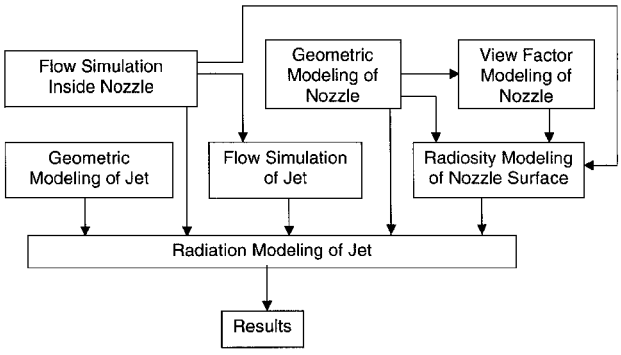

Fig. 2 Block diagram of computation scheme.

Modeling

As can be seen in Fig. 1, the missile sensor perceives different parts, shapes, and regions of the nonhomogeneous jet with different locations of itself with respect to the jet. These perceptions change not only with the orientation and location of the sensor with respect to the jet, but also with its field of view or aperture. For the side location (as in Fig. 1a) some of the rays or lines of sight emanate from the deep interior of the nozzle and pass through the homogeneous and nonhomogeneous parts of the jet. The remaining rays have a passage only through the jet. However, for the tail-on location (as in Fig. 1b), most of the radiation is due to the rays that emanate from the deep interior of the nozzle and pass through the jet. Finally, for the aft location (as shown in Fig. 1c), the jet radiation, as perceived by the sensor, does not have any direct contribution at all from the nozzle interior. Hence detailed flow simulations and exhaustive geometric/radiation modeling are required 1) for flow simulations inside the nozzle and its jet, 2) to identify and isolate parts of nozzle and jet contributing to radiation, 3) to determine radiation emanating from the jet, 4) to include the effect of nozzle interior radiation, if any, on some or all of this radiation, and 5) to account for effective perception of this radiation by the sensor for any of its given locations and orientations. The radiation modeling requires the flow properties inside the nozzle and jet as determined from flow simulation, whereas the geometric modeling requires the discretization of the jet region, the formation of discrete elemental panels and volumes and their identification for radiation contribution. Thus, this modeling scheme involves different aspects that form parts of a typical computation scheme as shown in Fig. 2.

Nozzle Internal Flow and Jet Development

The flow simulation has been made in two parts. The first part deals with the flow generation in the nozzle, which yields the exit conditions. The second part utilizes the nozzle exit conditions so derived as the initial conditions for the flow development outside.

Flow Simulation Inside Nozzle

As noted by Shapiro,[13] the one-dimensional approximation is very useful in the study of flow in ducts. Therefore, the flow inside the nozzle is assumed to be steady, one-dimensional, inviscid and isentropic, shock free, and chemically reacting. An existing code, namely that contained in a NASA report by Lordi et al.,[14] has been adapted for this purpose. The required details of program adaptation and modification made are found in Refs. 15 and 16. Because turbine fuels are made up of hundreds of different hydrocarbons, a simple molecular formula, C_8H_{18} of the form of C_nH_{2n+2} has been assumed for the fuel. The species proportions of the mixture obtained for combustion of this fuel in excess air can be easily computed from equilibrium considerations. Because the code does not deal with the combustion process per se, but considers all elemental reactions that make up the equilibrium, the stagnation temperature at the inlet of the nozzle is a prescribed parameter and not computed from combustion reactions. This is appropriate because substantial energy transfer would have already occurred during expansion through the turbine. The code examines only the downstream part, where species concentrations vary along with pressure and temperature as the flow expands through the nozzle. Because of the very small variations in actual magnitudes of the mass fractions of carbon dioxide and water vapor between equilibrium and frozen flows even for a stoichiometric mixture, flow analyses have been made only for frozen flow composition. Figure 3 shows the predicted variations of temperature, pressure, and Mach number for the flow with a fuel-to-air ratio of 0.0142 for a subsonic expansion. It can be seen that the temperature and pressure ratios at the throat are about 0.83 and 0.53, respectively, as predicted by isentropic flow theory. The expansion corresponds to a practical case because the nozzle exit pressure is about 1 atm. The shallow nozzle divergence, 0.05 deg, is reflected in the variations of pressure, temperature, and Mach number with distance because most of the variation takes place in the convergent part. IR signals of interest will be predicted later for practical cases such as this subsonic expansion and another supersonic expansion. The input data required for the code and the corresponding nozzle exit conditions derived out of them for these cases are given in Tables 1 and 2.

Table 1 Input data

Case	Type of flow	N_C [a]	N_H [a]	N_O [a]	N_N [a]	p'_O	T'_O
A	Subsonic flow, $F/A = 0.0142$ [b]	0.982	2.210	14.174	54.23	1.93	828.4
B	Supersonic flow, $F/A = 0.0172$ [b]	1.185	2.667	14.132	54.071	3.05	955.0

[a] Number of gram atoms of carbon, hydrogen, oxygen, and nitrogen per gram of mixture.
[b] Fuel-to-air ratio.

Table 2 Nozzle exit conditions

Case	Type of flow	Mass fraction of CO_2	Mass fraction of H_2O	p'_e, atm	T'_e K	U'_e m/s
A	Subsonic flow, $F/A = 0.0142$	0.043	0.020	1.1	716	493
B	Supersonic flow, $F/A = 0.0172$	0.052	0.024	0.96	705	740

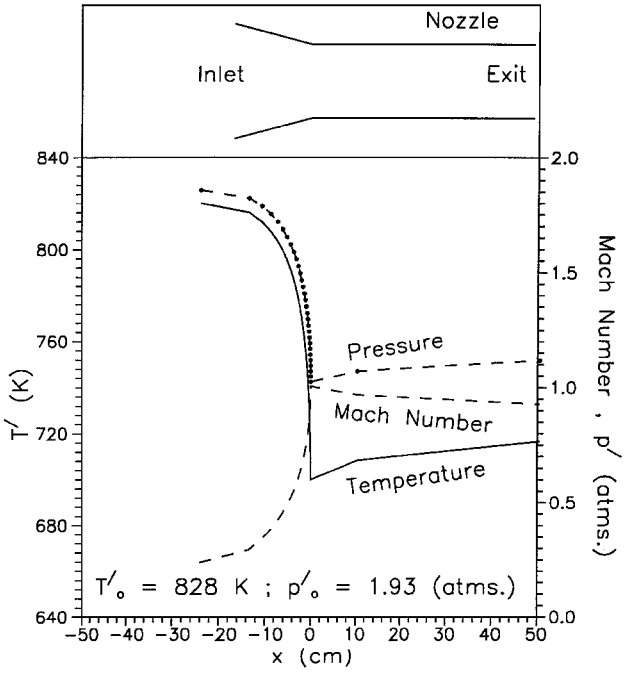

Fig. 3 Variations of temperature, pressure, and Mach number with distance along nozzle for subsonic expansion.

Flow Simulation Outside Nozzle

The flow outside nozzle or the jet is assumed to be steady, two-dimensional, viscous, nonreactive, compressible, and shock free.

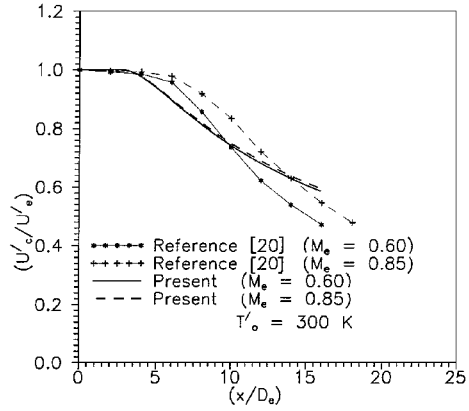

Fig. 4 Variation of nondimensional axial velocity in subsonic jets.

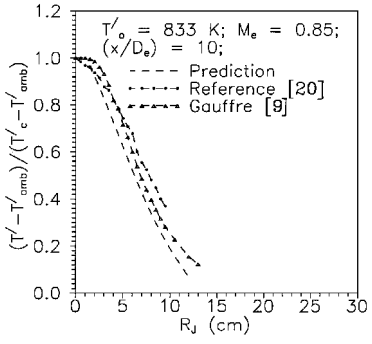

Fig. 5 Temperature profile across jet, $M_e = 0.85$.

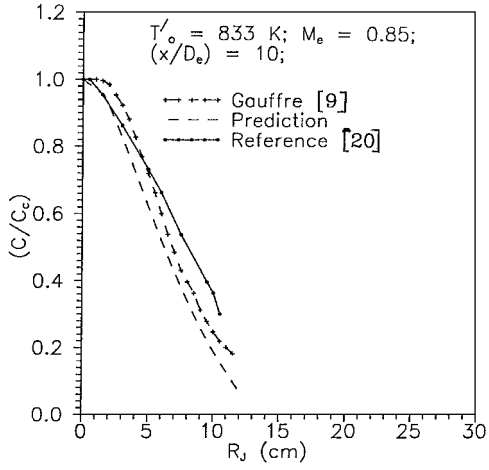

Fig. 6 Variation of carbon dioxide concentration across jet, $M_e = 0.85$.

The justifications for these assumptions made for flow simulations inside and outside nozzle may be found in Ref. 16. As explained by Abramovich,[17] a jet typically consists of an initial region mainly comprising the potential core, the transition region, and the developed region. Because the jets are boundary-layer-type flows, the GENMIX code, developed by Spalding[18] for boundary-layer-type flows, has been used for its simulation. The details regarding adaptation of the program are found in Ref. 19. The potential core is a region of high temperature and concentrations and will have a significant effect on IR signal emissions from the jet. Thus, in the present context of IR, the focus is on correct simulations of potential core and temperature and concentrations of CO_2 and H_2O. It was found that the mixing length parameter, in the computation of eddy viscosity, is an important tuning factor to obtain correct simulations of the potential core region. Hence, the flow simulations have been made based on the choice of mixing length parameter to yield a typical length of potential core for turbulent jets, which is about $6D_e$.

The simulation of optimally expanded flows has been validated against experimental results provided in Ref. 20 for both cold and hot jets. Air and a combusted mixture were used as the working media for the cold and hot jets, respectively. Based on the total temperature values, the fuel-to-air ratio was found to be 0.014 for the hot jet. Figure 4 shows the predicted variation of normalized axial velocity with distance for the case of cold jets. The local axial velocity has been normalized with respect to the nozzle exit velocity. Numerically predicted values in Fig. 4 show a fair agreement with the experiments, especially with respect to the constant region, indicating the good prediction of potential core. The axial variation of the normalized axial velocity shows invariance with Mach number, unlike the experiments. Note that the mixing length parameter has been set to a constant value in the prediction scheme and not as a function of downstream distance. Figure 5 shows the predicted variation of normalized temperature difference and Fig. 6 the predicted variation of normalized CO_2 concentration across the jet at an axial distance beyond the potential core, $x/D_e = 10$, in comparison with experimental values given in Ref. 20 and the values given by Gauffre.[9] The normalization has been done with respect to the centerline values and, hence, the variables assume a value of unity at the axis. It has been seen that the mismatch between predictions and experimental results can be corrected by using the mixing length parameter as a good tuning factor. However, it may happen at the expense of the accuracy of potential core region. The apparent flatness around the axis is due to low resolution at the center of the Gaussian curve. Thus, when the exit conditions of the internal flow simulations are used as input to the external flow, a reliable picture of the entire flowfield inside and outside the nozzle has been obtained.

Geometric Specifications

To tackle all IR scenarios, the nozzle, jet, and sensor are fixed arbitrarily in a three-dimensional coordinate system. The sensor is fixed in terms of the sensor center and the perpendicular to the sensor on its active side. The discretized points on the inside surface of the nozzle generated a priori are used. The jet is fixed in terms of the nozzle exit face center coinciding with the jet origin, any point on the nozzle axis and any point on the edge of initial jet section coinciding with the nozzle exit face, as indicated in Fig. 1. The parameters required for grid generation are N_{dg}, N_{sg}, k_g, $D(K)$, and $P(I)$, which provide wide flexibility in controlling the discretization. Furthermore, the species concentrations and the temperatures at each of these jet radii $P(I)$ at each of the $D(K)$ elemental distances along jet axis are obtained from flow calculations made earlier. Therefore, the values of N_{dg}, k_g, $D(K)$, and $P(I)$ have to be compatible with the GENMIX code employed for external flows. The nozzle inside surface as such can have varying temperatures and emissivities. These are explicitly specified based on practical values. The gaseous environment inside the nozzle obtained from internal flow calculations is assumed to be homogeneous and is equal to the exit conditions because very little variation occurs in the diverging section in view.

Generation of Grid Points

The generation of grid points in the jet domain is based on the solution of three equations, namely, 1) the equation for a point on a plane such as a jet section, 2) the equation for the dot product of two lines, and 3) the equation for the distance between two points on the plane. With the final solution being based on a single quadratic equation, the solution process needs to be carried out for only one-half of a section. Thus, $(N_{dg} \times N_{sg} + 1)$ number of grid points are generated on each section. To ensure a proper correspondence between the grid points on adjacent sections so that the grids do not become skewed, principles of coordinate geometry and linear algebra as described by Flanders and Price[21] have been used. With these specifications, it is possible to generate a total number of $[(N_{dg} \times N_{sg}) \times (3k_g + 1)]$ grid panels, which include $\{(N_{dg} \times N_{sg}) \times (k_g + 1)\}$ number of planar grid panels occurring on the nozzle face and jet sections and $(N_{dg} \times N_{sg} \times 2 \times k_g)$ number of planar grid panels between adjacent sections. As shown in Fig. 7, most of these grid panels are quadrilateral, such as abdc, with only a small number touching the

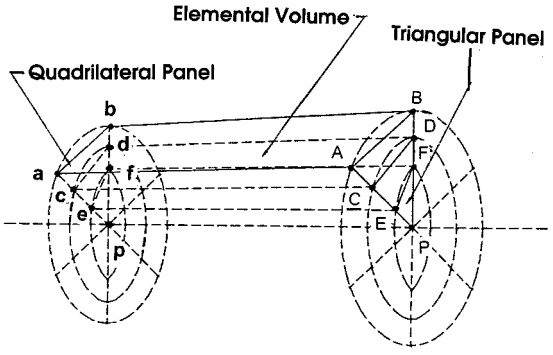

Fig. 7 Schematic of occurrence of panels and volumes between sections.

axis being triangular, such as efp. Most of the elemental volumes formed by these panels are six sided, such as abdcCDBA, with only a small number bounded by triangular panels being five sided such as efpPFE. The radiation from any elemental panel is assumed to originate from its centroid. Many subscripted variables are used like three-dimensional subscripted variables for centroids and grid points. For the centroids, the subscripts indicative of the angular, radial, and axial nature vary from 1 to $(2 \times N_{sg})$, 1 to N_{dg}, and 1 to $(2 \times k_g - 1)$, whereas for the grid points, the subscripts vary from 1 to N_{sg}, 1 to N_{dg}, and 1 to $(K_g + 1)$, respectively.

Identification of Columns Contributing to IR Signal

The uninterrupted lines of sight joining the sensor center with the centroids of some of these grid panels on the outer surface of the jet will form the centers of elemental gas columns that contribute to the radiation (shown in Fig. 8). The radiation contribution of each of these contributory elemental gas columns will sum up to the heat flux of radiation. The contributory elemental gas column, within which the sensor perpendicular lies, accounts for the intensity of radiation. The prime task of geometric modeling is to isolate the elemental gas columns that contribute to radiation.

In this task, it is first seen whether the sensor is located behind the nozzle face. If the angle ϕ as shown in Fig. 8a is $\leq$90 deg, the sensor is behind the nozzle face, the nozzle face does not contribute, and only the panels on the outer surface of the jet are considered for computational purposes. It has to be determined whether the line of sight and, hence, the radiation from some of these panels are also blocked by the nozzle face. Thus whether the line of sight joining the sensor center with the centroid of a panel intersects the plane of the nozzle face is examined. If the distance of this point of intersection from the nozzle center is less than the radius of the nozzle exit face, then the radiation from that panel is blocked, and it is disregarded. Otherwise, the panel is considered for further analysis. If $\phi > 90$ deg, the nozzle face may contribute, and all of the grid panels on the nozzle face are considered for their radiation contribution along with those on the jet.

Next for each of the panels under consideration, it is checked whether the angle α, as shown if Fig. 8b, is greater than 90 deg. A panel is disregarded if α is greater than 90 deg because the orientation of the sensor is such that its back is facing the panel like panel m shown in Fig. 8a. Otherwise that panel (like panel l, whose position is indicated in Fig. 8a) will be considered for IR computations.

Finally, it is seen whether angle β (Fig. 8b) is greater than 90 deg. If the angle is greater than 90 deg, the location of the panel is such that its back is facing the sensor and not otherwise. Invariably a near-end panel like k will be such that its back is facing the sensor, whereas a far-end panel like j will be such that its back will not (as in Fig. 8a). These tests result in the isolation of gas columns of lengths s and bounded by pairs of far-end and near-end panels. These columns determine the radiation signal.

For the gas columns starting from the nozzle face, it is necessary to determine the lengths of the gas columns within the nozzle interior that contribute to the radiation. The panels on the inside surface of the nozzle, containing their intersection points with the lines

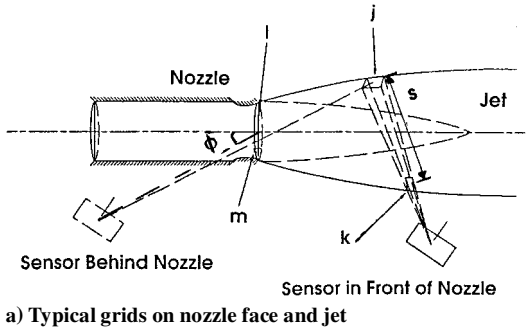

a) Typical grids on nozzle face and jet

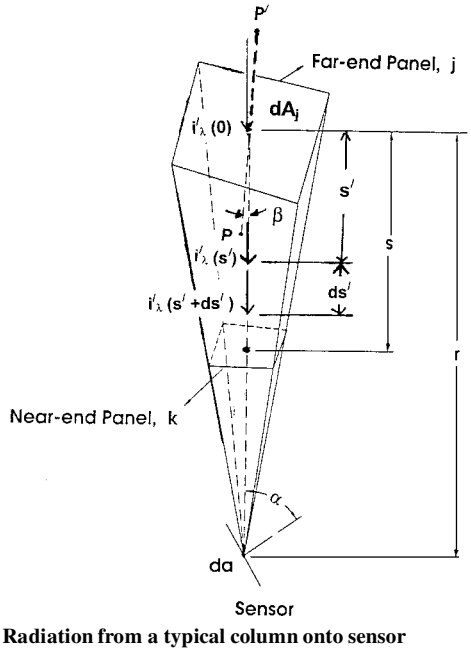

b) Radiation from a typical column onto sensor

Fig. 8 Occurrence and formation of grid panels and elemental volumes with respect to sensor.

of sight, are determined. The lengths of gas columns (between such intersection points on the inside surface of the nozzle and the nozzle exit face) contribute to radiation from the nozzle interior in addition to the radiosities of the panels on the inside surface of the nozzle where the lines of sight terminate. For the gas columns that have been isolated, the area of the far-end panel of this elemental gas column, dA_j, and the extent of the gas column within the jet, s, the angles α, β, and the distance of the far-end panel from the sensor center, r, are determined (Fig. 8b). These quantities are used in radiation calculations to be described later.

The computations described suffice for a homogeneous gas region. However, for a nonhomogeneous gas region, it is required to identify the gas conditions encountered along a ray or a line of sight. The gas conditions are assumed constant within an elemental volume formed by the grid panels but varying from one volume to the other. The same techniques of geometric modeling used for the homogeneous gas region are used for the nonhomogeneous gas region to isolate pairs of far-end and near-end panels and to find their intersection points with the line of sight that form elemental lengths ds' as shown in Fig. 8b. Each of these elemental lengths determine the extent of the local homogeneous gas conditions that determine the radiation signal. These elemental volumes, which do not occur in a descending or ascending fashion along the line of sight, are further shuffled. This effectively places the elemental volumes within each column in their naturally occurring order. The geometric modeling that has been developed requires many geometric computations for the generation of the planar equations of the grid panels, their centroids, and their perpendiculars directed into the gas region, as well as computation of their areas and determination of their intersection points with lines of sight, gas column lengths, panel distances from

the sensor, effective panel areas, and angles. These computational details are explained in Ref. 16.

It must be emphasized that the mass that contributes to the IR signal is a complex three-dimensional shape. Thus, although the jet is treated as a body of rotation from the two-dimensional case solved earlier, geometric modeling evolved here is essentially three dimensional and can be used for any arbitrary radiating medium or for any other property estimation.

Radiation Modeling

The radiation from a jet is dependent on its thermodynamic conditions, the species comprising the jet, its physical dimensions, and boundary conditions. The temperature determines the nature of radiation such as continuum or band radiation, which occurs at temperatures typical of jet engine exhausts, and the strength or intensity of radiation signal. Pressure exerts influence on radiation through a broadening mechanism. The species determine the radiation bands with each species having characteristic bands. The absorption coefficient and physical path length determine what is known as the optical path lengths, which determine the radiation strengths. The boundary conditions mainly occur as initial radiation incident on jet boundary as it happens on the nozzle face as in the case of a sensor viewing in a tail-on mode.

Computational Model

With reference to Fig. 8b, the basic radiative transfer equation given by Siegel and Howell,[22] in the absence of scattering, reduces to

$$\frac{\mathrm{d}i'_\lambda}{\mathrm{d}s'} = -a_\lambda i'_\lambda(s') + a_\lambda i'_{\lambda b}(s') \tag{1}$$

Equation (1) can be modified to yield the radiative transfer equation given in Ref. 23 in terms of transmissivity as

$$i'_\lambda(s) = i'_\lambda(0)\tau_\lambda(0, s) + \int_0^s i'_{\lambda,b}\frac{\partial}{\partial s'}\tau_\lambda(s', s)\,\mathrm{d}s' \tag{2}$$

The first term represents the effect of initial radiation and the second term represents the effect of radiation through the gas column on the total radiation.

The determination of spectral intensity requires the determination of spectral transmissivity, which requires the computation of optical path lengths. Optical path length is a misnomer in the sense that it is actually a nondimensional quantity. However, it is extensively used in radiative studies to indicate the attenuation along the path. The specification of absorption coefficient for different species and thermodynamic conditions and their application along the actual path lengths for the determination of optical path lengths and transmissivities is based on band models.

Band Models

Band models are hypothetical models of simplified structure, which are introduced to provide a fair representation of the radiation properties of real gases at a reasonable computing cost. In general, a model consists of a set of lines in a spectral interval with specified properties regarding the intensities, shape, number, and distributions of lines. Band models can be classified into narrowband models and wideband models. The two types of wideband models are the box model and the exponential wideband model of Edwards.[12] The types of narrowband models are Elsasser model and the statistical model. Because the wideband models are useful for obtaining total quantities and the narrowband models are useful for obtaining spectral information, the results based on the application of narrowband model given in Ref. 23 are presented here.

Narrowband Models

Reference 23 deals with the development of a narrowband model based on the Curtis–Godson approximation. This narrowband model considers both collision broadening and Doppler broadening. It is based on randomly spaced and equally intense collision and Doppler lines for collision and Doppler broadening. The present work considers the single line group form of the narrowband model given in Ref. 23 to yield the transmissivity to be used in Eq. (2). The spectral transmissivity of a medium containing a system of species is

$$\tau_\lambda = \exp\left[-\sum_i X_i\right] \tag{3}$$

The application of this band model for the detemination of optical path lengths requires the knowledge of the absorption coefficients and mean inverse line spacing for the species that are considered in radiation computation, namely, CO_2, H_2O, and CO. The data given in Ref. 24 have been used. The details of the adaptation of this narrowband model are given in Ref. 16.

The radiation through an elemental gas column, in terms of total intensity signal incident at the sensor location, is given by

$$i'(s) = \int_\lambda i'_\lambda(s)\,\mathrm{d}\lambda = \sum_\lambda i'_\lambda \Delta\lambda \tag{4}$$

whereas the heat flux signal is given by

$$q = \int\int_\lambda i'_\lambda\,\mathrm{d}\lambda\frac{\mathrm{d}A_j\cos\beta}{r^2}\cos\alpha$$

$$= \sum_j\left[\sum_\lambda i'_\lambda\Delta\lambda\right]\frac{\Delta A_j\cos\beta}{r^2}\cos\alpha \tag{5}$$

Numerical integration is carried out to solve for these signals, which require various geometric quantities such as angles, areas, and distances determined from geometric modeling.

When the sensor is viewing the nozzle in a tail-on mode, it requires to determine $i'_\lambda(0)$ of Eq. (2), to evaluate the initial radiation, which is the contribution from the nozzle interior. This is dependent on nozzle surface radiosities and the gas conditions inside nozzle because the nozzle interior contribution is assumed to originate at the nozzle exit face instead of its surface. This evaluation is based on the radiation modeling of the nozzle interior as will be explained.

Radiation Modeling of Nozzle Interior

Radiation from the nozzle interior emanates from the hot inside surfaces of the nozzle and traverses through the hot gas, which acts as a participating medium. The nozzle surface radiosities consist of the emitted and reflected portions of the radiated energy. The emitted portion is determined by the individual surface temperatures and their emissivities. The reflected portion is determined by the incident radiation and the surface reflectivities. However the incident radiation itself depends on the visibility of each of the other individual surfaces from the surface under consideration and the radiosities of those surfaces. Hence, the radiation from the nozzle interior is a typical example of gas radiation in an enclosure.

The hot gas inside the nozzle is assumed to be an absorbing and emitting medium with uniform properties equal to that of the potential core of the outside jet as noted earlier. A tail-on view of the nozzle shows a combination of surfaces, as shown in Fig. 9a. Because aircraft engine nozzles are fairly shallow as compared to, for example, rocket nozzles, it suffices to treat the nozzle and the inside portion as a cylinder, as shown in Fig. 9b, though it is possible to account for its actual outer shape. The head end of the cylinder is treated as a hot surface to account for the complex details inside. The cylinder length is set equal to the sum of the slant lengths of the nozzle or the sum of the jet pipe length and the slant lengths, and its fore and aft areas have been set equal to the nozzle exit face area. The nozzle inside surfaces are assumed as diffuse and gray with specified properties of temperature and emissivity. The grid points of the inside surface of the nozzle generated a priori are used in the formation of elemental triangular areas or panels, which make up the nozzle surface. Because the many reflections and radiations between the individual surfaces have a tendency to even out the directional dependencies of the radiation between the surfaces, the radiation results based on the diffuse and gray nature of the surfaces may not be much different from the realistic scenario. The radiation model

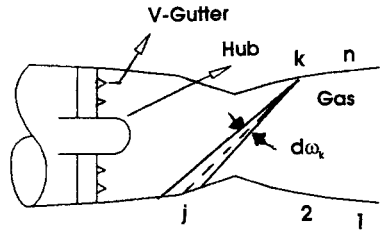

a) Actual tail-on-view

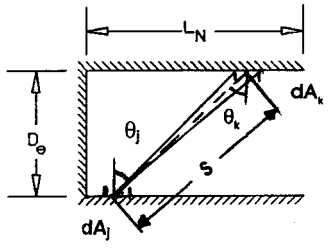

b) Idealized representation

Fig. 9 Schematic of nozzle.

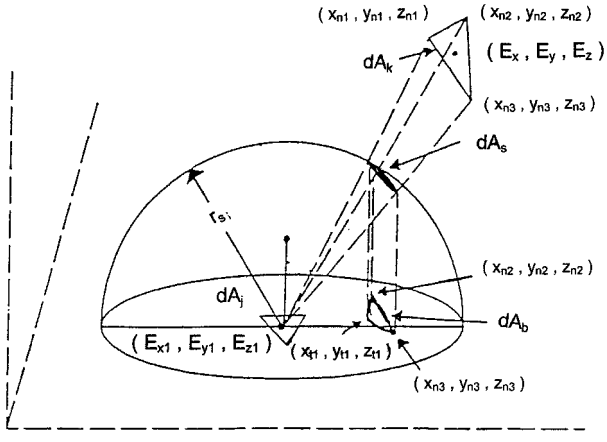

Fig. 10 Geometry of unit-sphere method for obtaining view factors.

considers the participation of the gas inside the nozzle, although the results have been generated in its absence.

The visibility of the panels with respect to one another is defined by the view factors of the panels. With respect to Fig. 9b, it is given by

$$\mathrm{d}F_{dj-dk} = \left(\frac{\cos\theta_j \cos\theta_k}{\pi s^2}\right) \mathrm{d}A_k \tag{6}$$

Most of the methods available in the literature for the computation of these view factors have their limitations in the form of convergence or requirement of excessive computer resources such as time and memory. An elegant method is the unit sphere method of Nusselt, which has been discussed by Siegel and Howell.[22] Its application can be understood with respect to Fig. 10. The method involves the construction of a hemisphere with one of the elemental areas $\mathrm{d}A_j$ as the center of the hemisphere. The other elemental area $\mathrm{d}A_k$ is first projected onto the hemisphere surface to form area $\mathrm{d}A_s$ and further onto the base to form area $\mathrm{d}A_b$, as shown in Fig. 10. Equation (6) reduces to

$$\mathrm{d}F_{dj-dk} = \left(\frac{\cos\theta_j}{\pi}\right) \mathrm{d}\omega_j = \frac{\mathrm{d}A_b}{\pi r_s^2} \tag{7}$$

Thus, the computation of view factors reduces to the determination of $\mathrm{d}A_b$. The general view has been that it is rather inconvenient to determine the projected areas on the hemisphere surface and its base. Thus, this technique has traditionally been the basis of only graphical and experimental methods, as noted by Siegel and Howell.[22] However, in the present work, a direct application of the unit sphere method of Nusselt has been attempted. Its numerical application has been possible using techniques of linear algebra. These view factors form a matrix, which is used in the radiation modeling scheme to form a modified matrix system for solution.

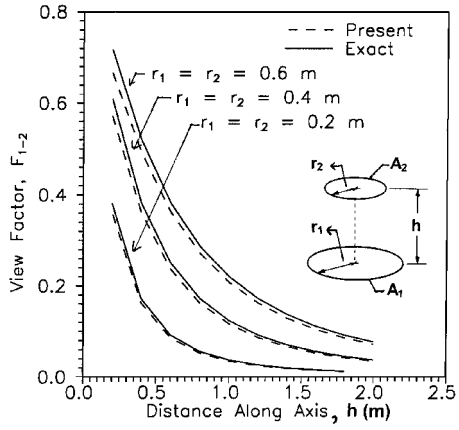

Fig. 11 Variation of view factor between parallel circular disks, $r_1 = r_2$.

Typical View Factor Results

Figure 11 shows the view factor results for a two-disk configuration. This configuration is similar to the geometric orientation of the front and aft ends of an aircraft engine nozzle, with respect to each other. As a validation case, the predicted variation of view factors with distance are shown for a range of disk sizes. This range encompasses the sizes of normal nozzle sections. Good agreement is noticeable in Fig. 11. The agreement improves with decreasing disk size and lower ratio disk radius to axial distance. The minor deviations may be because of numerical accuracy levels that result in the closure relation not being satisfied. Beyond a certain precision in view factors, it is more important to consider the uncertainty in radiation properties to get accurate results.

Radiation Formulation

Because the nozzle surface radiosities are dependent on each other, the formulation for the determination of these radiosities has to be a coupled system of equations. Consider an enclosure composed of n surfaces as shown in Fig. 9a. The outgoing spectral flux made up of emitted and reflected energy can be written for a diffuse gray surface as

$$\mathrm{d}q_{\lambda O,k} = \epsilon_k\, e_{\lambda B,k}\, \mathrm{d}\lambda + \rho_k\, \mathrm{d}q_{\lambda I,k} \tag{8}$$

Considering the participation of gas inside the nozzle, it can be shown that

$$\mathrm{d}q_{\lambda I,k} = \sum_{j=1}^{n} [\pi i'_{\lambda O,j} \tau_{\lambda,j-k}]\, \mathrm{d}F_{k-j}\, \mathrm{d}\lambda + \sum_{j=1}^{n} [e_{\lambda B,G} \alpha_{\lambda,j-k}]\, \mathrm{d}F_{k-j}\, \mathrm{d}\lambda \tag{9}$$

Equation (9) can be used to substitute for $\mathrm{d}q_{\lambda I,k}$ in Eq. (8) to yield

$$\begin{aligned} &-\pi\rho_k\tau_{\lambda,1-k}\,\mathrm{d}F_{k-1} i'_{\lambda O,1}\,\mathrm{d}\lambda - \pi\rho_k\tau_{\lambda,2-k}\,\mathrm{d}F_{k-2} i'_{\lambda O,2}\,\mathrm{d}\lambda - \cdots \\ &\quad + \pi i'_{\lambda O,k}\,\mathrm{d}\lambda - \cdots - \pi\rho_k\tau_{\lambda,n-k}\,\mathrm{d}F_{k-n} i'_{\lambda O,n}\,\mathrm{d}\lambda \\ &\quad = \epsilon_k e_{\lambda B,k}\,\mathrm{d}\lambda + \rho_k[e_{\lambda B,G}\alpha_{\lambda,1-k}\,\mathrm{d}F_{k-1}\,\mathrm{d}\lambda \\ &\quad + \cdots + e_{\lambda B,G}\alpha_{\lambda,n-k}\,\mathrm{d}F_{k-n}\,\mathrm{d}\lambda] \end{aligned} \tag{10}$$

In the absence of the participation of the gas inside the nozzle in the radiation process, the formulation reduces to

$$\begin{aligned} &-\pi\rho_k\,\mathrm{d}F_{k-1} i'_{\lambda O,1}\,\mathrm{d}\lambda - \pi\rho_k\,\mathrm{d}F_{k-2} i'_{\lambda O,2}\,\mathrm{d}\lambda - \cdots + \pi i'_{\lambda O,k}\,\mathrm{d}\lambda \\ &\quad - \cdots - \pi\rho_k\,\mathrm{d}F_{k-n} i'_{\lambda O,n}\,\mathrm{d}\lambda = \epsilon_k\, e_{\lambda B,k}\,\mathrm{d}\lambda \end{aligned} \tag{11}$$

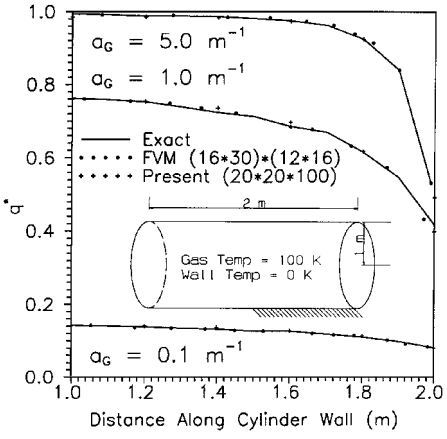

Fig. 12 Nondimensional heat flux on side wall of a cylindrical enclosure containing an absorbing, emitting, and nonscattering gas.

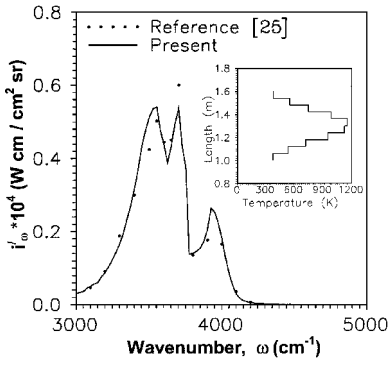

Fig. 13 Predicted variation of spectral intensity for nonisothermal column of CO_2, H_2O, and N_2.

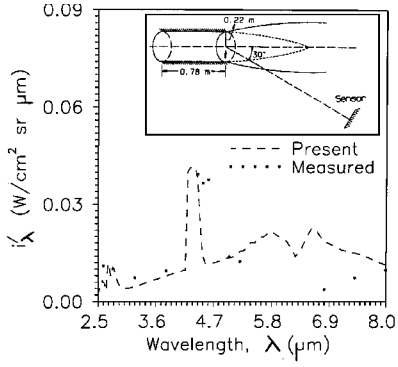

Fig. 14 Comparison of predicted and measured spectral intensities for actual engine.

The formulation results in a system of equations cast in a matrix form, the size of which is determined by the number of panels. Because the number of panels required in the analysis of practical problems is high, the size of this matrix is large. Hence, its inversion to determine the solution vector containing the radiosities of the panels is based on the Gauss–Siedel iteration procedure to obtain the results within a reasonable time. These radiosities form the initial radiation in the application of Eq. (2) for radiation from gas columns inside the nozzle. The radiation so obtained forms the initial radiation for the jet radiation as noted earlier. The details of view factor computations and radiation formulation are given in Ref. 16.

Results and Discussion

The combined code for geometric and radiation models is first validated against two well-known cases, one for heat flux and the other for spectral intensity, and later some predictions of practical interest have been made. Figure 12 shows the nondimensional heat flux predictions for an absorbing, emitting, and nonscattering gray gas obtained with fewer grids than the method of Chui et al.[6] The cylinder walls are black at 0 K (as shown in the inset) and do not participate in the radiation process. The heat flux incident only on one-half of the cylinder side wall is shown because the radiation environment is symmetric. The predominant effect of solid angle in heat flux computations is seen for all of the three cases of different absorption coefficients, with the heat flux being maximum at the center of the cylinder and a monotonic reduction in heat flux with distance from the center. These aspects are more pronounced when the gas medium has a high absorption coefficient.

Spectral Intensity

Figure 13 shows the spectral intensity predictions in comparison with that given by Simmons et al.[25] for radiation for a nonisothermal mixture of the two radiating species, CO_2 and H_2O with N_2. The partial pressures of H_2O, CO_2, and N_2 are 57, 28, and 675 mm of Hg, respectively. The temperature profile and pressure are similar to that found across a subsonic jet. The predicted spectrum covers the common peak regions (around 2.7 μm) of water vapor and carbon dioxide. The intensity peaks due to these have been predicted fairly well with respect to their locations. Apart from the possible differences in the absorption coefficient and line spacing data, the possible contributing factor for the slight mismatch in peak values at some locations may be the difference in accounting for the inhomogeneities along the line of sight.

Spectral Intensity Predictions for Engine Exhausts

Radiation measurements made on a ground-based aircraft gas turbine are available in Ref. 26. In the absence of sufficient details, the nozzle exit gas temperature is estimated to be around 635 K, the exit pressure to be around 1 atm, and the nozzle wall temperature to be about 500 K, based on thermodynamic cycle and heat transfer considerations. A wall emissivity value of about 0.8 is assumed. The expected values of mass fractions of carbon dioxide and water vapor are around 0.042 and 0.02, respectively, roughly corresponding to case A in Table 2. A mesh of (39 × 20 × 100) has been used in the computations. Because the jet is axisymmetric, a small number of grids for the angular direction is not likely to have any significant effect on the predictions. For the nozzle inside surface, a total of 410 grid points as used resulting in a total number of 780 triangular panels for which the surface radiosities were computed. The predictions from the present model as shown in Fig. 14 compare reasonably well with the measured data, especially at shorter wavelengths. The important peaks at about 2.7 and 4.3 μm corresponding to gas radiation due to CO_2 and H_2O and nozzle surface radiation at about 5.8 μm have been predicted well. There is no transfer of energy from one wavelength band to another wavelength band. The small disagreement at shorter wavelengths and the mismatch at the longer wavelengths between the prediced values and the measured data may be due to the approximations in modeling of the nozzle interior radiation. Note that the variation of gas temperature inside the nozzle has not been considered, whereas all of the panels of the nozzle wall have been set to the same emmissivity. In addition, the empirical expression given in Ref. 24 for H_2O spacing is based on a binary mixture. An intensity calculation of this nature takes a typical time of about 120 min on the IBM 3090 (Model-150E) computing system. Most of this time is required for the computation of nozzle wall radiosities.

Heat Flux for Optimum Expansions

Figure 15 shows the polar plot of heat flux for the supersonic case, namely, case B in Table 2. The same mesh as for the earlier calculation has been use in the generation of this polar plot. The sensor opening is assumed to be completely wide (half-angle being 90 deg), whereas the locus of sensor movement is as shown in the inset. The generation of heat flux results is computationally intensive. Hence, these results have been genereated on a RS/6000 (Model-58H) system. It takes about 1500 min to generate the results for

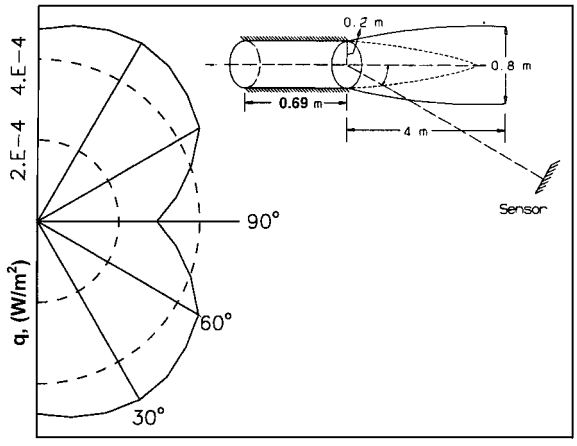

Fig. 15 Polar plot of heat flux for supersonic expansion.

20 locations of the sensor over a polar angle of 180 deg. Figure 15 shows the symmetrical nature about the jet axis with the heat flux signal being a minimum in the tail on mode. Thus, the nozzle radiation has a deterministic effect only on intensity. The signal variation with increasing angle from the jet axis is because of the variation in solid angle subtended at the sensor by the radiating gas volume.

Conclusions

The complexities in terms of the combination of surface and gas radiation, the inhomogeneites of the medium, and the complicated geometry of the radiating volume comprising the jet and nozzle make the task of predicting IR signal a difficult but an interesting engineering problem. The practical need to have such a signal predicted for any arbitrary sensor location and orientation makes it more involved. Indeed, the geometric variations arising with sensor position become critical at close ranges in this context. The present work has attempted to model the problem of IR signal prediction covering all of its facets.

References

[1]Hottel, H. C., and Sarofim, A. F., *Radiative Transfer*, McGraw–Hill, New York, 1967, pp. 354–357.

[2]Lockwood, F. C., and Shah, N. G., "A New Radiation Solution Method for Incorporation in General Combustion Prediction Procedures," Eighteenth Symposium (International) on Combustion, Combustion Inst., Pittsburgh, PA, 1981, pp. 1405–1414.

[3]Steward, F. R., and Cannon, P., "The Calculation of Radiative Heat Flux in a Cylindrical Furnace Using the Monte Carlo Method," *International Journal of Heat and Mass Transfer*, Vol. 14, No. 2, 1971, pp. 245–262.

[4]Gosman, A. D., Lockwood, F. C., and Salooja, A. P., "The Prediction of Cylindrical Furnaces Gaseous Fueled with Premixed and Diffusion Burners," 17th Symposium (International) on Combustion, Combustion Inst., Pittsburgh, PA, 1979, pp. 747–760.

[5]Abou Ellail, M. M. M., Gosman, A. D., Lockwood, F. C., and Megahed, I. E. A., "Description and Validation of a Three Dimensional Procedure for Combustion Chamber Flows," *Turbulent Combustion*, edited by L. A. Kennedy, Vol. 58, Progress in Astronautics and Aeronautics, AIAA, New York, 1978, pp. 163–190.

[6]Chui, E. H., Raithby, G. D., and Hughes, P. M. J., "Prediction of Radiative Transfer in Cylindrical Enclosures with the Finite Volume Method," *Journal of Thermophysics and Heat Transfer*, Vol. 6, No. 4, 1992, pp. 605–611.

[7]Chai, J. C., Parthasarathy, G., Lee, H. S., and Patankar, S. V., "Finite Volume Radiative Heat Transfer Procedure for Irregular Geometries," *Journal of Thermophysics and Heat Transfer*, Vol. 9, No. 3, 1995, pp. 410–415.

[8]Decher, R., "Infrared Emissions from Turbofans with High Aspect Ratio Nozzles," *Journal of Aircraft*, Vol. 18, No. 12, 1981, pp. 1025–1031.

[9]Gauffre, G., "Aircraft Infra-Red Radiation Modeling," *La Recherche Aerospatiale*, No. 4, 1981, pp. 21–41.

[10]Ludwig, C. B., Malkmus, W., Freeman, G. N., Slack, M., and Reed, R., "A Theoretical Model for Absorbing, Emitting, and Scattering Plume Radiation," *Spacecraft Radiative Transfer and Temperature Control*, edited by T. E. Horton, Vol. 83, Progress in Astronautics and Aeronautics, AIAA, New York, 1982, pp. 111–127.

[11]Docherty, P., and Fairweather, M., "Predictions of Radiative Transfer from Nonhomogeneous Combustion Products Using the Discrete Transfer Method," *Combustion and Flame*, Vol. 71, No. 1, 1988, pp. 79–87.

[12]Edwards, D. K., "Molecular Gas Band Radiation," *Advances in Heat Transfer*, Vol. 12, Academic Press, New York, 1976, pp. 115–193.

[13]Shapiro, A. H., *The Dynamics and Thermodynamics of Compressible Fluid Flow*, Vol. 1, Wiley, New York, 1953, pp. 73, 74.

[14]Lordi, J. A., Mates, R. E., and Moselle, J. R., "Computer Program for the Numerical Solution of Nonequilibrium Expansions of Reacting Gas Mixtures," NASA CR-472, May 1966.

[15]Heragu, S. S., "Implications of Nozzle Flow Solver for IR Signature Studies," Aeronautical Development Agency, Rept. ADA/TD/SA/020, Bangalore, India, Dec. 1989.

[16]Heragu, S. S., "A Generalized Model for Infrared Perception from an Engine Exhaust," Ph.D. Dissertation, Indian Inst. of Science, Bangalore, India, May 1997.

[17]Abramovich, G. N., *The Theory of Turbulent Jets,* M. I. T. Press, Cambridge, MA, 1963, pp. 3, 4.

[18]Spalding, D. B., *GENMIX: A General Computer Program for Two-Dimensional Parabolic Phenomena*, Vol. 1, Pergamon, Oxford, England, U.K., 1977.

[19]Heragu, S. S., "Application of GENMIX to Jet Flow Simulation," Aeronautical Development Agency, Rept. ADA/LCA/TD/SA/005, Bangalore, India, March 1988.

[20]Krishnamoorthy, V., and Pai, B. R., "Aerothermodynamics and Infrared Emission Characteristics of Simulated Aeroengine Jet Plumes," Propulsion Div., Project Document PR 9113, National Aeronautical Lab., Bangalore, India, July 1991.

[21]Flanders, H., and Price, J. J., *Calculus with Analytic Geometry*, Academic Press, New York, 1978.

[22]Siegel, R., and Howell, J. R., *Thermal Radiation Heat Transfer*, 2nd ed., McGraw–Hill, New York, 1981.

[23]Ludwig, C. B., Malkmus, W., Reardon, J. E., and Thomson, J. A. L., *Handbook of Infrared Radiation from Combustion Gases*, NASA SP-3080, 1973.

[24]Huffaker, R. M., and Dash, M. J., "A General Program for the Calculation of Radiation from an Inhomogeneous, Nonisobaric, Nonisothermal Rocket Exhaust Plume," NASA TM X-53622, June 1967.

[25]Simmons, F. S., Yamada, H. Y., and Arnold, C. B., "Measurement of Temperature Profiles in Hot Gases by Emission–Absorption Spectroscopy," NASA CR-72491, April 1969.

[26]Murthy, A. N., and Kulkarni, H. D., "Report on Infra Red Spectral Emission Measurements on Scaled Model Engine and Jaguar Aircraft Engine Plumes," Defence Electronics Research Lab., Rept. DLRL : R : 91 : 026, Hyderabad, India, April 1991.